

CoMPLEX

University College London

Mini Project 2

Freeze Drying of Medicine

Dimitrios Voulgarelis

Supervisors: Prof Frank Smith & Prof Ajoy Velayudhan

Abstract

In the current project a discussion is given regarding freeze-drying or lyophilization with specific interest in its application to the storage of pharmaceutical products. Moreover, a number of important mathematical and computational models in the field of freeze-drying are presented, with the main focus being placed on their differences, uses, conclusions and evolution from the first simple models to more sophisticated ones and back again to simpler models for different purposes. Finally, the last part of the project is an original mathematical approach for the description of the freezing stage of lyophilization, using the Cauchy Integral formulation.

Contents

1	Lyophilization	2
2	Modelling The Freeze-Drying Process	5
2.1	Freeze-Drying in Trays	6
2.2	Freeze-Drying in Vials	8
3	Mathematical Description of The Small Time Behaviour of The Freezing Stage in Vials	11
3.1	Top and Side Layers	12
3.2	Top Corners	13
3.3	Bottom Corners	16
3.4	Full Model	17
A	Latent Heat Boundary Condition After Conformal Mapping	21
B	Leading Order Approximation of Integrals In The Two Limit Cases	23
C	Asymptotic Limits of Θ, Ψ On The Corner's Sides	25

Chapter 1

Lyophilization

Lyophilization or Freeze-Drying is defined as a stabilizing process [20] (removal of solvent) where initially the substance is frozen and then dried, first by sublimation and later by desorption, until the moisture reaches low levels that prevent reactive and degradative processes. There are several advantages to this type of drying over others. The most important and relevant to complex medicines (macromolecules) is that drying of the solvent occurs at low temperature without excessive heating that could denature the proteins. Further advantages include lower transportation costs since, removing solvent means removing weight, reduced oxidative denaturation since the product is sealed in low vacuum or inert gas, easy reconstitution by adding diluents [20], highly controlled environment, increase of storage life as well as very low water content at the end of the process. A different preservation method was freezing preservation which came with very high transportation costs due to large weights and the possibility of total loss in the case of malfunctioning of the freezing plant. Hence, both the advantages of freeze-drying and the disadvantages of freeze preservation led a lot of people to the study and adoption of the first. Pharmaceutical products are usually stored in vials with a stopper on top to seal the product after the process.

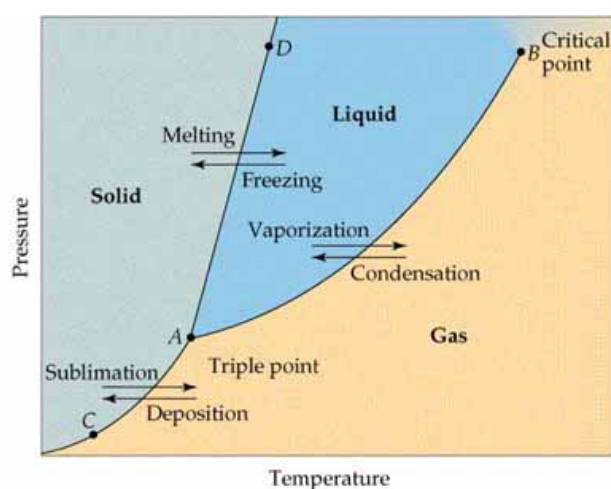


Figure 1.1: Phase diagram showing the triple point threshold A. In order to avoid the liquid state the partial water pressure must stay below that point [3].

The lyophilization process is constituted of three stages (Figure 1.2 [3]). The first stage is the freezing of the product. During this stage the temperature of the product is lowered in order to go from the liquid to the solid state. The type of freezing (rate of freezing) can directly affect the product quality and is considered to be very important since it affects the crystalline structure (size/shape of the crystals) of the frozen product which in turn affects the drying stage. On the one hand, higher rates usually produce small crystals, which prolong the drying times due to the high resistance of vapor flow while lower rates produce large crystals that minimize the resistance to moisture [], but on the other hand slow freezing can cause decrease of the pH of some forms of sodium phosphate resulting in decreased stability of the frozen and freeze-dried drug and it can also cause cold denaturation of certain proteins [17]. It is worth noticing that a few other factors control the form of this structure, other than the freezing rate. Such factors are the nature of the product as well as the processing before the freezing. Depending on the nature of the product the freezing must proceed below a critical temperature. For crystalline material that temperature is the Eutectic temperature whereas for an amorphous mix it is the Glass Transition temperature. In the case of an incomplete freezing there is the danger of foaming (melt back) when low vacuum is applied and hence of product deterioration [2]. During freezing not all water is removed but some remains as bound/adsorbed water.

Following the complete freezing of the product, the second stage starts which is called the primary drying stage. At this stage the pressure is dropped below the triple point, as seen in Figure 1.1 [3], in order to avoid the liquid state and for sublimation to occur. Constant heating needs to be applied to the product, since sublimation causes energy/temperature loss (latent heat loss). So, without sufficient heat the product will cool which will result in an extension of the drying time. Heating control is vital during the primary drying stage for a number of reasons. Besides the prolonging of drying times, due to insufficient heat, too much heat could mean melting (foaming) and hence result in an unacceptable product. The general constraint is that the temperature of the frozen product must not exceed the critical temperature mentioned before and although this might not be too difficult for products stabilized by crystalline materials (eutectic temperature is high), proteins and peptides require different excipients with much lower critical temperatures. Another essential control parameter is the pressure. As already mentioned, the partial water vapor pressure needs to be constantly maintained below the triple point. Moreover, the partial pressure surrounding the product must be lower than the partial pressure of the ice itself for evaporation to occur [2]. Hence, decreased pressure leads to increased evaporation but below a certain value a further decrease in pressure will not improve evaporation but will act as a barrier to heat transfer [2]. Primary drying is the longest stage and a main reason behind that is the fact that the migration of the vapor is a diffusion process. This stage ends when all ice has sublimed and only the bound moisture remains. A small amount of bound water is removed during primary drying but the majority is removed in the next stage.

The third and final stage of lyophilization is the secondary drying stage where the chemically bound water is reduced to the desired level to enhance stability. After the end of the primary drying stage the moisture is still at relatively high levels 7-8% [3]. During

the secondary drying the temperature of the product is raised, while staying again below the constraints and the pressure is further dropped. The end product moisture levels are usually between 1-3%.

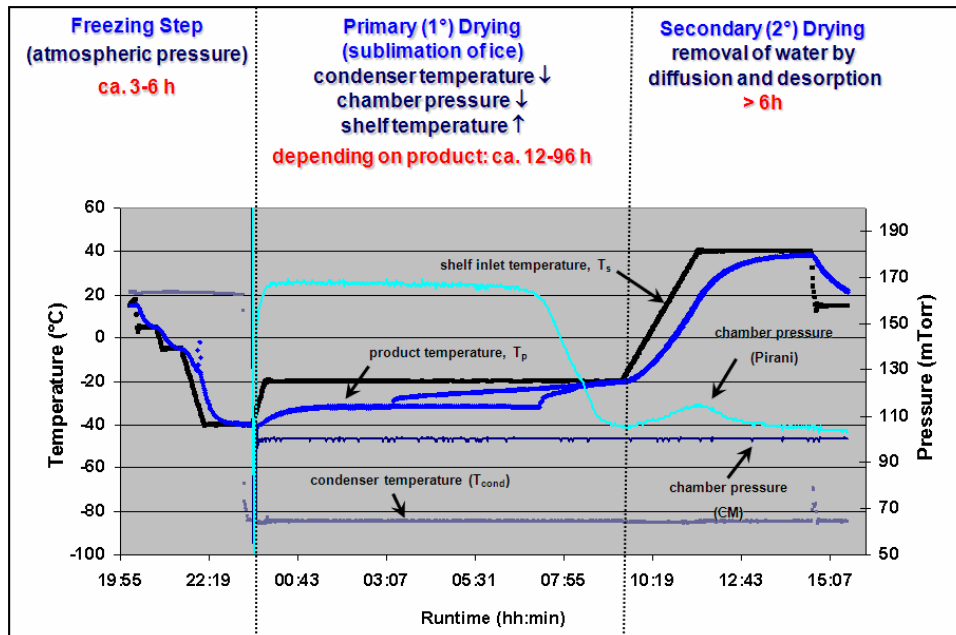


Figure 1.2: Pressure and temperature changes throughout the freeze-drying process [3].

Chapter 2

Modelling The Freeze-Drying Process

The freeze-drying method gained a lot of ground and is extensively used in other industries besides the pharmaceutical (e.g food industry). The high cost of the process and the long times made the need for modeling imperative in order to gain better understanding and identify the optimal operational conditions. These can be approached by different methods. These are trial and error and later sequential analysis where the design of an experiment is determined by the results of the previous. The approaches mentioned give no answers as to the cause of the observed behaviors; therefore experiments must be designed where the effect of altering single factors is explored [5]. Experiments on the changes of single factors can be very time consuming however. As a result many researchers used mathematical and computational modeling to tackle these problems.

Modeling lyophilization has several advantages and can have different uses depending on its nature. The main benefit is that it can provide insight into the dynamics of freeze-drying and thus enhance understanding of the underlying physics. Also, mathematical and computational models can be used for both off-line and on-line optimization. Off-line optimization can identify the optimal operational conditions while on-line can provide a means to monitor the main parameters and make corrections in real time conditions. Hence, these models help professionals make better decisions and can potentially reduce both time and cost and improve product quality [5]. The nature of the model plays a crucial role as to how it can be used effectively. So, the form of the model is directly linked to its purpose. There are complex 2D and 3D models that depend on many parameters and can describe the phenomenon better and more realistically, but cannot be used for real time applications or if they become too complex they might not even be able to enhance understanding. Moreover, there are simplified models essential for routine application [5] but there is the danger of oversimplification which could lead to results that are not realistic or useful. Finally, a basic factor as to the use of the model is whether or not its predictions are important indicators of product quality [5]. Models whose predictions are such, can be used for the development of tools of lyophilization cycles [5].

A number of models have been created to describe freeze-drying starting from very simple and moving to more complex ones that take into consideration previously ignored

factors. The first models were 1D and described freeze-drying in trays whereas the later models were 2D and described the process in vials, some taking into account the nature of the vial and its position in a shelf of the freeze-drier.

2.1 Freeze-Drying in Trays

One of the first models describing the freeze-drying process was the non-steady state heat and mass transfer model derived by Liapis & Litchfield [11]. It was used as an optimal control model where, with the use of a quasi steady state analysis, they found some general operational policies for decreasing the process time. The control parameters of the optimal control model were the chamber pressure and the radiator energy output. In their 1D model the frozen product of thickness L is placed on a tray where heating is provided from above. The equations describing the process are energy balances of the frozen and dried regions, continuity equations and fluxes. A number of assumptions were made, with the most characteristic for this model being that sublimation occurs parallel to the surface of the sample and that the side and bottom are perfectly insulated. After the derivation of the full model the conditions for optimality were derived using variational calculus. In order to derive the analytical solution of these conditions they solved the quasi-steady state version of the model. For the optimization part, four different cases were considered based on two constraints. The system constraints were that the surface temperature must not exceed a specific value called scorch temperature, T_s , of the dried product and the interface must not exceed the melting temperature, T_m . Then, the four cases were (i) neither constraint is active, (ii) surface temperature constraint active, (iii) interface temperature constraint active and (iv) both constraints active. Their analysis of the four cases indicated that initially both the pressure and the heat flux must be at their maximum value until the interface constraint is reached where the pressure must be dropped so as to keep the interface temperature at its maximum value without crossing the critical temperature. Then, the heat input must also be reduced to keep the surface temperature from exceeding the scorch temperature. To summarize, their work indicates that an optimal operational policy is to run the process very close to the constraints, which is something that will be found to be a very important policy in later modeling papers. It is important to notice that in their model no bound water removal was considered, which occurs during primary drying, and that their results are found under the assumption of quasi-steady state.

The two authors created a model based on the previous one with the same assumptions but including the removal of bound water during the primary drying stage [14]. In their improved model they allow for the occurrence of sublimation and desorption at the same time. After deriving the equations the problem needed to be implemented numerically since an analytical solution was not possible. To this end, they used a specific non-dimensionalization to immobilize the moving boundary and then solved numerically using the Crank-Nicholson method. They simulated the drying of turkey meat and tested the validity of their model against experimental data. Their results were in good agreement and predicted the drying time to acceptable accuracy. It is worth mentioning that

using these models, Litchfield, Liapis & Farhadpour checked the hypothesis that cyclical pressure (periodically varying chamber pressure) can improve the drying times []. What they found was that although that policy reduced the process time, an operational policy near an optimum value for the pressure gave consistently better results and required minimum equipment [13],[12].

Moving on from models that only account for heating from the top, Millman et al. [16] presented an 1D sorption-sublimation model where heat is provided independently both from the top and the bottom plates and tested it against different operational policies to find the one which produces the shortest time. In their model heat is also provided from the sides but its effect is considered negligible with respect to the top and bottom and is hence ignored and in contrast to the previous model, removal of free and bound water does not occur simultaneously but one starts after the other has terminated. Moreover, a very important aspect of their work was the development of bound water profiles which is useful both for quality control and process termination. In this model the same assumptions and numerical methods were used as for the previous model. Four cases were considered, each with each own plate conditions and with varying sample thickness and chamber pressure and the simulation was conducted for skim milk. Skim milk contains enzymes and proteins and hence it is very often used as it can be considered a complex pharmaceutical product. Their results indicate that the policy which achieves the shortest overall time is the one that gives the shortest free water removal phase. Furthermore, the largest heat and mass fluxes are achieved at policy C where the material constraints are both active (T_s and T_m). Finally, the sorbed water profiles produced from the model are essential for predicting and minimizing quality deterioration [16].

In the context of freeze-drying in trays, there were two other models developed in order to describe the dynamics of both drying stages (primary, secondary) for pharmaceuticals. The first model was the one developed by Liapis & Bruttini [10]. The purpose of this model was to derive a mathematical model describing the dynamics of the drying stages so as to analyze the drying rates which determine the drying time. Regarding the formulation, heat is supplied from every direction but again the side heating is considered negligible and the assumptions remain the same. Two large sets of equations were derived, that represent the two stages and the model was simulated and validated for skim milk and cloxacillin monosodium salt which are both considered amorphous solutes. The agreement with the experimental data was good for both stages and pointed towards three rate controlling mechanisms for the removal of bound water in the secondary stage: (i) desorption of bound water, (ii) mass transfer of water vapor by convection through the dried material pores, and (iii) Knudsen and bulk diffusion of water vapor in the pores. The second model, developed by Sadikoglu & Liapis [22], was based on the equations and assumptions of the previous one. In the current formulation the dusty- gas model was used to describe the transport of solvent vapor through the dried material pores. The benefit of using this approach is that no details are needed for the structure of the pores. A number of very interesting results were found from this model. The first is that the effect of neglecting the removal of bound water during the primary stage did not introduce a significant error. Moreover, as far as the mass transfer mechanisms are concerned, during the secondary drying stage, convective flow through the porous structure

was found to be insignificant for the determination of the dynamic behavior of this stage, but they pointed out that this mechanism should not be ignored until further a number of theoretical and experimental results suggested so.

2.2 Freeze-Drying in Vials

Following the development of 1D models describing freeze-drying in trays, multi-dimensional models were developed that described freeze-drying in vials. These models offered a more realistic representation of the process and were also concerned with a very important factor not present before, the position of the vial in the freeze-drier shelf.

The first 2D simulation of freeze-drying in vials was conducted by Mascarhenas et al. [15]. The main limitations of 1D models addressed in this papers was the fact that rectangular materials were required and the interface had to be planar and parallel to the base, hence not a curved shape. 2D mass and heat transfer phenomena were considered and the interface could be of arbitrary shape and the arbitrary Lagrangian-Eulerian scheme was used for tracking the sublimation interface. This scheme allows for the formulation of a moving reference frame using a finite-element mesh consisting of grid points in arbitrary spatial motion. The 2D mesh keeps changing throughout time to incorporate for the thickness change of the frozen and dried region. As a result, the current model overcame the limitations of 1D models and was used to describe both drying stages of skim milk and BST. The results obtained were in accordance to previously published results and provided information about the position and shape of the interface.

Sheehan & Liapis [24] constructed a 2D unsteady state model for the description of the dynamic behavior of the two drying stages and tested it against different operational policies. Regarding the previous model by Mascarhenas et al. [15] a number of problems were identified and improved on in this paper. The main problem is that it fails to provide correct times for the drying stages because it does not account for cases were the interface does not extent all the way along the diameter of the vials. A very important feature of the model was the use of the side heat, which is the source of radial effects, since it was pointed out that these effects are vital for correct 2D modeling. Moreover, a reference was made to the difference in the condition of vials in different locations along the freeze-drier shelves and they concluded that this phenomenon can be modeled with the use of single vial models subjected to different, position dependent, conditions. In their model primary and secondary drying coexist during the primary drying regime with the first being mainly active in the centre, while the latter in the outer annular volume element. Their results though indicated that the effect of desorption is negligible during the primary stage, as was already pointed out in previously. For the numerical solution a new set of variables was chosen so as to immobilize the moving boundary and the method of orthogonal collocations was used. The equations were simulated for skim milk in three cases. In the first case the vial is positioned in the outer array of vials on the shelf and the plate temperature is kept at the highest allowed values. In the second case the vial is again positioned in the outer array but with the temperature of the plate at a constant value and finally in the third case the vial is in the centre with the same temperature

policy as the first case. After the completion of the primary stage the temperature is set at the scorch temperature constraint. The shortest time was found for case I and the slowest for case II. This result points towards a more aggressive policy close to the temperature constraints. The authors noticed that a single temperature control profile cannot be used for the whole array of vials without violating the constraints in some of the vials, hence there is the need for modeling all vials as a whole and not separately for different conditions. Finally, they concluded that aggressive control of the temperature, near the constraints, offers faster times and more uniform temperature and bound water distributions.

On 2002 Brulls & Rasmuson [6] created a theoretical model that systematically described heat transfer in vials. In their model they included effects, previously neglected, such as heat accumulation in the vial, curvature of the vial bottom. Then, this heat transfer model was used to develop a lyophilization model that was simulated to test the influence of a number of factors (fullness, bottom curvature, position of the shelf, glass vial) and compared against experimental data. This resulted in a very comprehensive study of freeze-drying in vials. In their model the heat from the bottom of the vial was in the form of radiation due to the curvature of the vial base, and it was observed that this curvature had influence on the temperature that was correlated to pressure. For pressure above a certain value this influence is significant but not so for pressure below that value. This is very different to most of the previous models where the transfer of bottom heat was through conduction. Also, different from other models is the fact that no heat was considered from the top of the vials since their stopper acts as an insulator. Furthermore, they noticed that there was a great difference between the shelf and vial temperature for corner vials, due to heat transfer from other sources (sides), but no difference for the center vials. Finally, the dynamics due to the shape of the vial cannot be ignored since they found that heat accumulation plays a major role especially for low levels of fullness which is relevant for pharmaceutical products [6].

As seen from previous models the position of the vial is very important and the radial effects introduced from the sides are not negligible. Later models, based on earlier models, explored the effect of sides more systematically. Sadikoglu et al. [23] extended a model discussed earlier [22] for freeze-drying in trays to include 2D effects and heat from top bottom and sides and designed an optimal control model for freeze-drying and found policies that reduced the total time markedly. What their results showed was that the optimum result is obtained from running the process close to the temperature constraints and keeping the pressure at its minimum values to increase water vapor flux, hence an optimum value for the pressure. Also, very interesting was their finding that one of the factors of optimum control is minimizing the heat transfer from the sides. This result was further supported by Gan et al. [8] who used the model by Sheenan & Liapis [24] to explore the effect of the tray sides in freeze-drier shelves. They tested three cases one of which was with no sides. They found that this case gave the shortest times and the most uniform distribution of bound water and of water loss. Their results also suggested that the chamber walls should operate in a temperature slightly higher than the melting temperature during primary stage and slightly lower than the scorch temperature during secondary stage.

In order to optimize the primary drying stage of freeze-drying in vials, both with off-line optimization and on-line monitoring and control, Velardi & Barresi [25] developed a very detailed one-dimensional model. Due to the complexity and the high number of equations this model was unsuitable for on-line use and therefore, two simplified models were also developed based on the more complex one. Initially, they simulated vials placed in the center of the vial array and thus shielded from side heating, using the detailed model. The results were in good agreement with experimental data from freeze-drying cycles. Then, having this model as a starting point they developed the two simplified models. For the first model, heat and mass transfer was considered stationary due to slow process and the heat was only supplied from the bottom. Also, heat transfer was not considered in the dried layer. This model was not suitable for corner vials since it assumed insulated sides. The second simplified model is more complex than the first since heat transfer is considered for both the dried and frozen layers. Heat and mass transfer are again stationary and heat from the environment is still ignored. It is very interesting to notice that there was a very good agreement between the detailed and the second simplified model. Both simplified models allowed for analytical solutions and their simplified nature made them very useful for control and monitoring purposes and since their first appearance they have been widely used for the development of model-based tools for the freeze-drying cycles [5].

Going beyond the modeling of the two drying stages, there have been a few attempts to model the freezing stage so as to improve the stage. Bruttini et al. [7] conducted an exergy analysis and tested different policies to find the one that produces the least exergy losses. Their results suggested that a distribution of temperatures of the cooling source has significant benefits. Apart from reduction in exergy losses, a distribution of temperatures can produce good freezing rates that form continuous and highly connected crystals. A further modeling of the freezing stage was developed by Hottot et al. [9] who used the commercial finite element code FEMLAB. The advantage of using FEMLAB is that the real geometry of the vial can be drawn and used for real expressions of the boundary conditions. Their model was in accordance to the experiments they conducted.

Concluding this chapter about modeling freeze-drying we saw that the overwhelming majority of the models are concerned with the drying stages and little attention has been paid to the freezing stage, despite its evident importance for the whole process [5]. The modeling of the drying stages seems to be very useful and serve its purpose by not only providing insight into the process but also by guiding experiments and finding ways of optimization and time reduction. Modeling in the field of freeze-drying is far from complete as there are new technologies that can be used more effectively with the use of models. Such technologies include alternative sources of energy to improve heat transfer and dehydration rates (e.g. microwaves, infrared radiation, and radiofrequency), not yet used for pharmaceutical due to product restrictions, and addition of biological solvent to the water [5]. Finally, as already mentioned there is a great deal of unexplored modeling space for the freezing stage.

Chapter 3

Mathematical Description of The Small Time Behaviour of The Freezing Stage in Vials

The main focus of this chapter is the modeling of the small time regime of the freezing stage in a 2D rectangular vial, using a "Cauchy Integral Form" formulation of the governing equation. A reason behind the interest in the small time approximation is to check whether this formulation provides a valid basis for the complete solution of the problem which is then derived using the same approach. For general times the problem for the temperature between the vial walls and the interface, between the solid and liquid states, is a Stefan (moving boundary) problem given by the heat equation along with the appropriate non-dimensionalized boundary conditions. Thus

$$\nabla^2\Theta(x, y, t) = \beta^{-1}\partial_t\Theta. \quad (3.1)$$

Where, β is the latent heat over the heat capacitance of the solidified phase. In this case β^{-1} can be treated as a large number and the problem solved to first order, using perturbation theory, as Laplaces equation $\nabla^2\Theta(x, y, t) = 0$. This approach is justified and tested by Riley et al. [21], whose asymptotic solution was in good agreement to numerical work that included the right hand side term of (3.1). Hence, in the remainder of this work we shall consider Laplaces equation as the governing equation.

Here, $\Theta = 0$ on the top and side walls ($x = -1/2, x = +1/2, y = H$), $\Theta = 1$ on the floor ($y = 0$) and in the liquid region, including the interface, and finally taking into account latent heat we have $\frac{\partial\Theta}{\partial n} = \frac{g_t}{(g_x^2 + g_y^2)^{1/2}}$ on the unknown interface given by $g(x,y,t) = 0$.

Our goal is to find the temperature inside the frozen region as well as the unknown interface for small times. To this end we assume that for very small times the interface will take a nearly rectangular form, similar to the vial, with very thin top and side layers and with the bottom corners connecting to the vial's walls, as shown in Figure 3.1, due to boundary condition on the floor. The width of the vial is normalised to be equal to unity with the origin situated in the centre of the floor.

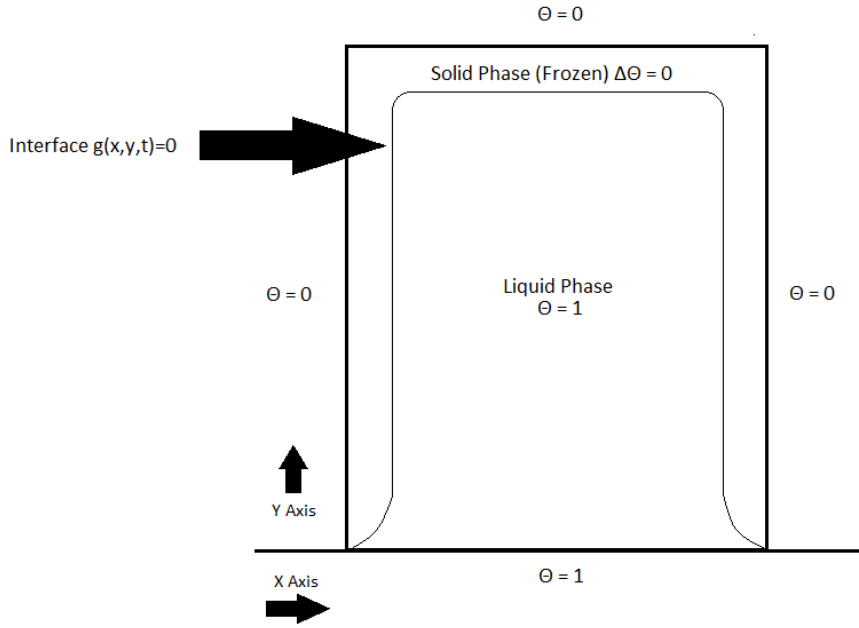


Figure 3.1: Shape of the interface during freezing for small times and the boundary conditions imposed on every side of the vial.

3.1 Top and Side Layers

Regarding the top and side layers, we assume that for small times they are very thin ($H - y \ll 1$ for the top layer and $x \pm 1/2 \ll 1$ for the side layers) and hence the $2D$ heat equation becomes $1D$ since the y or x derivative dominates, to first order approximation, in each case respectively. Furthermore scale analysis of the last boundary condition indicates that the thickness of the layer is of $O(t^{1/2})$ for $t \ll 1$. To see this consider the top layer. Taking $g \sim y$ and $\Theta \sim 1$ the last boundary condition yields:

$$\frac{\partial \Theta}{\partial n} = \frac{g_t}{(g_x^2 + g_y^2)^{1/2}},$$

$$\frac{1}{y} \sim \frac{y}{t}.$$

Hence, the appropriate scaling for small times is $y \sim t^{1/2}$. Using these simplifications we derive below the equations for the temperature and the thickness of the layers.

For the top layer we define the thickness G as $H - y$. Considering the time scaling, G and Θ can be expanded in orders of $t^{1/2}$ to get:

$$G = t^{1/2}G_0 + G_1 + \dots, \quad (3.2)$$

$$\Theta = \Theta_0 + t^{1/2}\Theta_1 + \dots \quad (3.3)$$

To get rid of t dependence a new variable is set as $y^* = \frac{y-H}{t^{1/2}}$. Hence, from (1.2) and from the definition of G we have $y^* = -G_0$. The new equation and boundary conditions for the temperature are $\partial_{y^*}^2 \Theta_0 = 0$, $\Theta_0 = 0$ for $y^* = 0$, $\Theta_0 = 1$ for $y^* = -G_0$ and $\frac{\partial \Theta_0}{\partial y^*} = -\frac{1}{2}G_0$ for $y^* = -G_0$, all to leading order. The last boundary condition can be derived by taking g to be equal to the leading order of G and noticing that the normal derivative w.r.t. to y must have opposite sign to the normal derivative w.r.t. y^* . From these it is trivial to show that $G_0 = 2^{1/2}$ and hence the equations for temperature and thickness are:

$$G = (2t)^{1/2} + G_1 + \dots, \quad (3.4)$$

$$\Theta = -\frac{y-H}{(2t)^{1/2}} + t^{1/2}\Theta_1 + \dots \quad (3.5)$$

Following exactly the same procedure but defining x^* as $x^* = \frac{x \pm 1/2}{t^{1/2}}$ the same equations are derived for the side layers with G_0 equal to $2^{1/2}$ again.

The situation is more complicated in the case of the corners. In those regions the heat equation must be solved for both y^* and x^* , of order unity, and it has to match asymptotically the solutions for the thin layers. Also the interface shape is completely unknown and cannot be taken as a constant to first order as before. Hence, a new approach must be used to tackle the corners. To this end the problem will be formulated using the Cauchy Integral Form so as to provide some equations that can be implemented numerically/computationally to verify their validity.

3.2 Top Corners

The first step in modeling the freezing stage at the top corners of the vial for small times is a conformal mapping from the initial plane, $z = x^* + iy^*$, to a new plane $Z(X, Y) = z^2$. The advantage of this mapping is that the X axis is a known boundary ($\Theta = 0$) and the unknown interface is a curve on the upper half plane, as shown in Figure 3.2.

In this new plane the relation between the x^*, y^* and X, Y is given by the following equations:

$$X = x^{*2} - y^{*2}, \quad (3.6)$$

$$Y = 2x^*y^*. \quad (3.7)$$

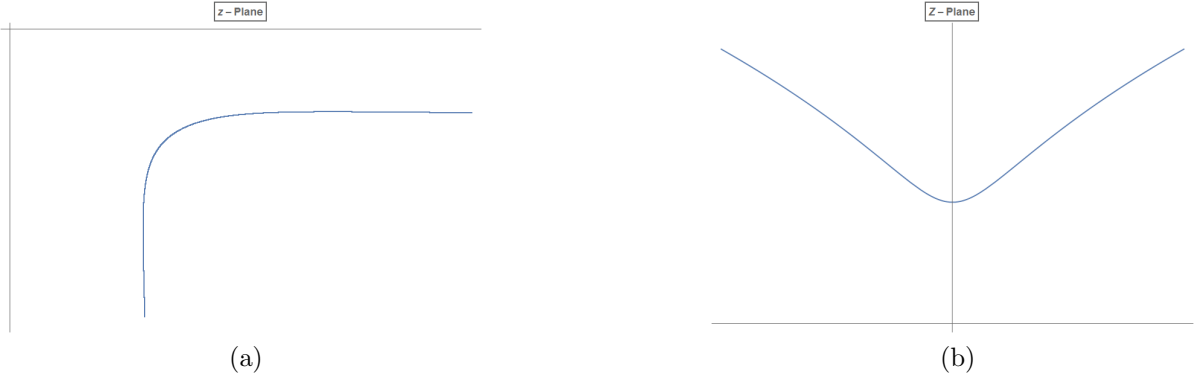


Figure 3.2: (a) Right top corner of the interface situated in the lower quadrant in the original z plane with x^* and y^* coordinates. (b) The interface corner after the mapping to the Z plane with X and Y coordinates

As a result of the mapping the last boundary condition (latent heat) is subject to alterations. The first thing to consider is that the left hand side, $\frac{\partial \Theta}{\partial n}$, is not equal to $\frac{\partial \Theta}{\partial N}$, where N is the normal to the interface in the Z plane. Furthermore, in the rhs of the equation the partial derivatives of g w.r.t. to x^* and y^* must be replaced with partial derivatives w.r.t. X and Y . For the sake of clarity the full derivation can be found in Appendix A. The resulting equation for the latent heat boundary condition in the new plane is as follows:

$$\frac{\partial \Theta}{\partial N} = -\frac{Xg_X + Yg_Y}{4(X^2 + Y^2)^{1/2}(g_X^2 + g_Y^2)^{1/2}}. \quad (3.8)$$

In order to use the Cauchy Integral form let us take a function Ψ which is related to Θ by $\Psi_Y = \Theta_X$. Taking the X derivative in both sides of this equation and using the fact that Θ satisfies the heat equation we get $\Psi_{XY} = -\Theta_{YY}$. Integrating w.r.t. Y leads to the second relation $\Psi_X = -\Theta_Y$. These two relations can be identified as the Cauchy-Riemann equations and we can now define a function $P(Z)$ such that, $P(X,Y) = \Theta(X,Y) + i\Psi(X,Y)$. Finally, by taking a closed contour in the Z plane, containing the unknown interface $Y = F(X)$ as seen in Figure 3.3, the Cauchy Integral along its boundary represents the value of the function $P(Z)$ inside that contour, where $q = \xi + i\eta$.

$$P(Z) = \int_C \frac{P(q)}{q - Z} dq. \quad (3.9)$$

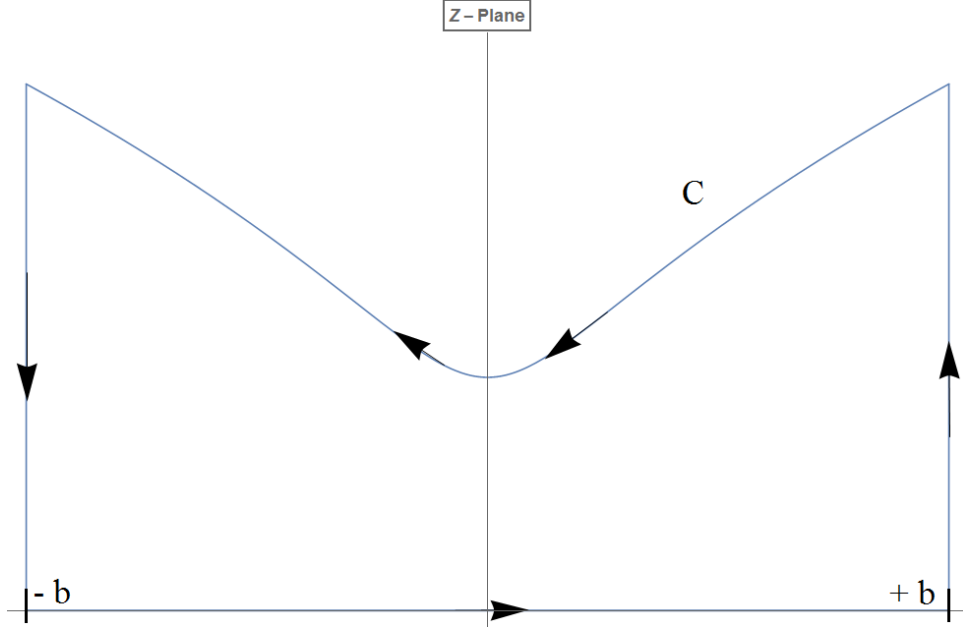


Figure 3.3: Contour C in the complex Z plane containing the unknown interface, the known boundary on the X axis and the two sides, a distance b from the origin, where Θ approaches asymptotically its solution for the top and side thin layer.

C can be broken down to four sub-contours. The first is the contour along the X-axis where $\eta = 0$, $dq=d\xi$ and $\Psi = \Psi_0(\xi)$. For the second and fourth contours which are the side contours, $\xi = \pm b$, $dq=d\eta$ and Θ, Ψ are functions of $(\pm b, \eta)$. In this case these functions will be represented by $\Theta_{s1,2}, \Psi_{s1,2}$ and their form is found using equation (3.5) in the new coordinate system (X,Y) and the relation between Θ and Ψ . The third contour goes along the unknown boundary where $\eta = F(\xi)$ and hence $dq = d\xi + i\frac{d\eta}{d\xi}d\xi = d\xi(1+iF'(\xi))$. Also, on that contour $\Theta = 1$ and $\Psi = \Psi_1(\xi)$. In order to find the equations necessary for the validation of this approach we take the imaginary part of (3.8).

$$\Psi(X, Y) = \text{Im}\left(\frac{1}{2\pi i} \int_{-b}^b \frac{i\Psi_0(\xi)}{\xi - X - iY} d\xi\right) + \text{Im}\left(\frac{1}{2\pi i} \int_0^{F(b)} \frac{\Theta_{s1}(b, \eta) + i\Psi_{s1}(b, \eta)}{b + \eta - X - iY} d\eta\right)$$

$$\text{Im}\left(\frac{1}{2\pi i} \int_b^{-b} \frac{1 + i\Psi_1(\xi)}{\xi + iF(\xi) - X - iY} d\xi\right) + \text{Im}\left(\frac{1}{2\pi i} \int_{F(-b)}^0 \frac{\Theta_{s2}(-b, \eta) + i\Psi_{s2}(b, \eta)}{-b + \eta - X - iY} d\eta\right)$$

$$\Psi(X, Y) = \frac{1}{2\pi} \int_{-b}^b \frac{i\Psi_0(\xi)Y}{(\xi - X)^2 + Y^2} d\xi - \frac{1}{2\pi} \int_0^{F(b)} \frac{\Theta_{s1} * (\eta - Y) - \Psi_{s1} * (b - X)}{(b - X)^2 + (\eta - Y)^2} d\eta$$

$$+ \frac{1}{2\pi} \int_{-b}^b \frac{(\xi - X)(1 - F'\Psi_1) + (F - Y)(F' + \Psi_1)}{(\xi - X)^2 + (F - Y)^2} d\xi + \frac{1}{2\pi} \int_0^{F(-b)} \frac{\Theta_{s2} * (\eta - Y) + \Psi_{s2} * (b + X)}{(b + X)^2 + (\eta - Y)^2} d\eta$$

The final step towards deriving the desired equations is using the previous result and considering two cases. In the first case $Y \rightarrow 0$ and $\Psi(X, Y) \rightarrow \Psi_0(X)$. In the second case

$Y \rightarrow F(X)$ and $\Psi(X, Y) \rightarrow \Psi_1(X)$. Caution is needed when treating the integrals in these two cases so as to find the correct leading order contribution. So, taking the two limits and using the final boundary condition, which using the Cauchy-Riemann equations can be expressed as $\frac{\partial \Theta}{\partial N} = -\frac{\partial \Psi}{\partial S}$, we arrive at a system of three equations for three unknowns (F, Ψ_1, Ψ_0). The partial derivative of Ψ w.r.t. the tangential direction, S , can be easily rewritten as a partial derivative w.r.t. X from the fact that $dS^2 = dX^2 + dY^2$. A full derivation of Θ_s and Ψ_s as well as the special treatment of the integrals involved in the two above mentioned limit situations can be found in Appendix B,C respectively.

$$\begin{aligned} \Psi_1(X) = & F'(X) + \frac{1}{\pi} F(X) \int_{-b}^b \frac{\Psi_0}{(\xi - X)^2 + F(X)^2} d\xi - \frac{1}{\pi} \int_0^{F(b)} \frac{\Theta_{s1} * (\eta - F) - \Psi_{s1} * (b - X)}{(b - X)^2 + (\eta - F(X))^2} d\eta, \\ & + \frac{1}{\pi} \int_{-b}^b b \frac{1 - F' \Psi_1}{\xi - X} d\xi + \frac{1}{\pi} \int_0^{F(b)} \frac{\Theta_{s2} * (\eta - F) + \Psi_{s2} * (b + X)}{(b + X)^2 + (\eta - F(X))^2} d\eta. \end{aligned} \quad (3.10)$$

$$\begin{aligned} \Psi_0(X) = & \frac{1}{\pi} \int_{-b}^b \frac{(\xi - X)(1 - F' \Psi_1) + F(F' + \Psi_1)}{(\xi - X)^2 + F(\xi)^2} d\xi - \frac{1}{\pi} \int_0^{F(b)} \frac{\Theta_{s1} \eta - \Psi_{s1} * (b - X)}{(b - X)^2 + \eta^2} d\eta, \\ & + \frac{1}{\pi} \int_0^{F(b)} \frac{\Theta_{s2} \eta + \Psi_{s2} * (b + X)}{(b + X)^2 + \eta^2} d\eta. \end{aligned} \quad (3.11)$$

$$\Psi_1'(X) = \frac{XF'(X) - F(X)}{4(X^2 + F(X)^2)^{1/2}}. \quad (3.12)$$

3.3 Bottom Corners

In order to derive the equations for the top corners we follow the same steps, regarding the function $P(z)$, but a conformal mapping is not needed in this case since the problem is simple enough. Taking as an example the left bottom corner, there are a few differences to the top corner. The contour is obviously different and now the interface $g(x^*, y^*)=0$ will be given by $g(x^*, y^*) = x^* - f(y^*)$, hence on the interface $x^*=f(y^*)$. The new contour, c , can be broken into three parts. The first part is the vertical line $h \rightarrow 0$ for $x^*=0$, where $dq=d\eta$, $\Theta = 0$ and $\Psi = \Psi_0$. The second part consists of the interface and here $dq = d\eta(i+f(\eta))$, $\Theta = 1$ and $\Psi = \Psi_1$. The last part is the horizontal line from $f(h) \rightarrow 0$ where $dq=d\xi$, and Θ_s, Ψ_s are functions of (ξ, h) . Taking again the imaginary part for the two limit cases, $x^* \rightarrow 0$ and $x^* \rightarrow f(y^*)$, as well as the latent heat boundary condition, we get the following three governing equations, their full derivation is very similar to the one found in Appendix B for the top corners and will be omitted:

$$\begin{aligned} \Psi_1(y^*) = & -f'(y^*) + \frac{1}{\pi} \int_0^h \frac{\Psi_0 f(y^*)}{f(y^*)^2 + (\eta - y^*)^2} d\eta + \frac{1}{\pi} \int_0^{\sqrt{2}} \frac{1 + f' \Psi_1}{\eta - y^*} d\eta \\ & + \frac{1}{\pi} \int_0^{\sqrt{2}} \frac{\Theta_s * (\xi - f) + \Psi_s * (h - y^*)}{(\xi - f)^2 + (h - y^*)^2} d\xi \end{aligned} \quad (3.13)$$

$$\Psi_0(y^*) = \frac{1}{\pi} \int_0^{\sqrt{2}} \frac{f(\Psi_1 - f') + (\eta - y^*)(1 + f'\Psi_1)}{f^2 + (\eta - y^*)^2} d\eta + \frac{1}{\pi} \int_0^{\sqrt{2}} \frac{\Theta_s \xi - \Psi_s * (h - y^*)}{\xi^2 + (h - y^*)^2} d\xi \quad (3.14)$$

$$\Psi_1'(y^*) = -\frac{1}{2}(f(y^*) + f'(y^*)y^*) \quad (3.15)$$

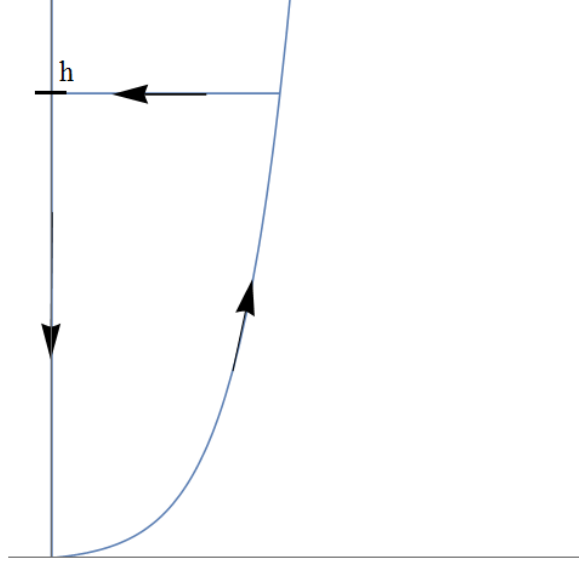


Figure 3.4: Contour c in the complex z plane containing the unknown interface, the known boundary on the y^* axis and top, a distance h from the origin, where Θ approaches asymptotically its solution side thin layer.

3.4 Full Model

The above equations for the corners can be tested by implementing them numerically and constructing an iterative process by making an initial guess for the interface function (F, f) and then recalculating it using the expressions for Ψ_1 and Ψ_0 . This was not conducted for this project but it can provide a good starting point for a later project. To derive the corresponding equation for the full problem for the time $O(1)$ the same procedure is followed. A contour is defined at the z -plane, Figure (3.5), and taking the imaginary part of the complex function $P(x, y)$ and the limits $y \rightarrow 0$ and $y \rightarrow f(x, t)$ gives the three equations. The goal is to find an expression for the unknown (latent heat) boundary condition for Θ . The three equations are given below, following a derivation almost identical to the previous equations.

$$\begin{aligned} \Psi_0^{(\beta)}(x, t) = & -\frac{1}{\pi} \int_{-1/2}^{1/2} \frac{(1 - f'\Psi_1)(\xi - x) + (\Psi_1 + f')f}{(\xi - x)^2 + f^2} d\xi - \frac{1}{\pi} \int_{-H}^0 \frac{\Psi_0^{(\alpha)}\eta}{(1/2 - x)^2 + \eta^2} d\eta, \\ & + \frac{1}{\pi} \int_{-H}^0 \frac{\Psi_0^{(\gamma)}\eta}{(1/2 + x)^2 + \eta^2} d\eta. \end{aligned} \quad (3.16)$$

$$\begin{aligned} \Psi_1(x, t) = & f'(x, t) - \frac{1}{\pi} \int_{-1/2}^{1/2} \frac{1 - f' \Psi_1}{\xi - x} \xi - \frac{1}{\pi i} \int_{-H}^0 \frac{\Psi_0^{(\alpha)}(\eta - f)}{1/2 - x)^2 + (\eta - f)^2} d\eta, \\ & - \frac{1}{\pi} f(x, t) \int_{-1/2}^{1/2} \frac{\Psi_0^{(\beta)}}{(\xi - x)^2 + f^2} d\xi + \frac{1}{\pi} \int_{-H}^0 \frac{\Psi_0^{(\gamma)}(\eta - f)}{1/2 + x)^2 + (\eta - f)^2} d\eta. \end{aligned} \quad (3.17)$$

Finally, using the initial latent heat boundary condition (for the non-scaled coordinates) and the relation between Θ and Ψ , as was used before, we get:

$$\frac{\partial \Psi_1(x, t)}{\partial x} = f_t(x, t). \quad (3.18)$$

Solving this system of equations could potentially give us the unknown boundary condition on the interface and hence allow for the full solution of the temperature using the heat equation (3.1). An analytical solution is not possible and thus this has to be carefully implemented numerically taking into account the fact that there are Principal value integrals. This approach seems promising and once it has been validated by numerical calculation it can be used to predict the temperature distribution during the freezing stage, any asymmetries of the process as well as the total time, all very vital information.

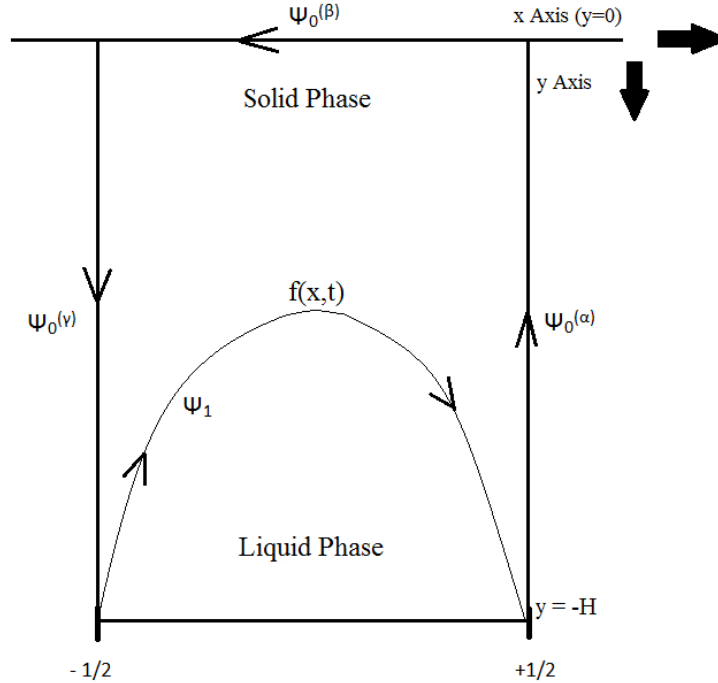


Figure 3.5: Contour for the full problem in the complex z plane containing the unknown interface f and the known boundary along the walls of the vial.

Bibliography

- [1] General Principles of Freeze Drying.
- [2] General principles of freeze drying (the lyophilization process). <http://freezedrying.com/freeze-dryers/general-principles-of-freeze-drying/>.
- [3] A short introduction:the basic principle of freeze drying. <http://www.freeze-drying.eu/html/introduction.html>.
- [4] Luis T. Antelo, Stphanie Passot, Fernanda Fonseca, Ioan Cristian Trelea, and Antonio A. Alonso. Toward Optimal Operation Conditions of Freeze-Drying Processes via a Multilevel Approach. *Drying Technology*, 30(13):1432–1448, October 2012.
- [5] Antonello Barresi and Roberto Pisano. Recent advances in process optimization of vacuum freeze-drying. *AMERICAN PHARMACEUTICAL REVIEW*, 17(3):56–60, 2014.
- [6] Mikael Brlls and Anders Rasmuson. Heat transfer in vial lyophilization. *International Journal of Pharmaceutics*, 246(1):1–16, 2002.
- [7] R. Bruttini, O. K. Crosser, and A. I. Liapis. EXERGY ANALYSIS FOR THE FREEZING STAGE OF THE FREEZE DRYING PROCESS. *Drying Technology*, 19(9):2303–2313, September 2001.
- [8] K.H. Gan, R. Bruttini, O.K. Crosser, and A.I. Liapis. Freeze-drying of pharmaceuticals in vials on trays: effects of drying chamber wall temperature and tray side on lyophilization performance. *International Journal of Heat and Mass Transfer*, 48(9):1675–1687, April 2005.
- [9] Aurlie Hottot, Roman Peczalski, Sverine Vessot, and Julien Andrieu. Freeze-Drying of Pharmaceutical Proteins in Vials: Modeling of Freezing and Sublimation Steps. *Drying Technology*, 24(5):561–570, June 2006.
- [10] A.I. Liapis and R. Bruttini. A theory for the primary and secondary drying stages of the freeze-drying of pharmaceutical crystalline and amorphous solutes: comparison between experimental data and theory. *Separations Technology*, 4(3):144 – 155, 1994.
- [11] Athanasios I. Liapis and Rod J. Litchfield. Optimal control of a freeze dryeri theoretical development and quasi steady state analysis. *Chemical Engineering Science*, 34(7):975 – 981, 1979.

- [12] R. J. Litchfield, F. A. Farhadpour, and A. I. Liapis. Cyclical pressure freeze drying. *Chemical Engineering Science*, 36(7):1233–1238, 1981.
- [13] R. J. Litchfield, A. I. Liapis, and F. A. Farhadpour. Cycled pressure and near-optimal pressure policies for a freeze dryer. *International Journal of Food Science & Technology*, 16(6):637–646, 1981.
- [14] R. J. Litchfield and Athanasios I. Liapis. An adsorption-sublimation model for a freeze dryer. *Chemical Engineering Science*, 34(9):1085–1090, 1979.
- [15] W.J. Mascarenhas, H.U. Akay, and M.J. Pikal. A computational model for finite element analysis of the freeze-drying process. *Computer Methods in Applied Mechanics and Engineering*, 148(12):105 – 124, 1997.
- [16] M. J. Millman, A. I. Liapis, and J. M. Marchello. An analysis of the lyophilization process using a sorption-sublimation model and various operational policies. *AIChE Journal*, 31(10):1594–1604, 1985.
- [17] Thomas W Patapoff and David E Overcashier. The importance of freezing on lyophilization cycle development. *BIOPHARM-EUGENE-*, 15(3):16–21, 2002.
- [18] Roberto Pisano, Davide Fissore, and Antonello A Barresi. In-line and off-line optimization of freeze-drying cycles for pharmaceutical products. *Drying Technology*, 31(8):905–919, 2013.
- [19] Roberto Pisano, Davide Fissore, Antonello A. Barresi, and Massimo Rastelli. Quality by Design: Scale-Up of Freeze-Drying Cycles in Pharmaceutical Industry. *AAPS PharmSciTech*, 14(3):1137–1149, September 2013.
- [20] Dejan S Pržić, Nenad Lj Ružić, and Slobodan D Petrović. Lyophilization: The process and industrial use. *Hemijaska industrija*, 58(12):552–562, 2004.
- [21] DS Riley, FT Smith, and G Poots. The inward solidification of spheres and circular cylinders. *International Journal of Heat and Mass Transfer*, 17(12):1507–1516, 1974.
- [22] H. Sadikoglu and A. I. Liapis. Mathematical Modelling of the Primary and Secondary Drying Stages of Bulk Solution Freeze-Drying in Trays: Parameter Estimation and Model Discrimination by Comparison of Theoretical Results With Experimental Data. *Drying Technology*, 15(3):791–810, 1997.
- [23] H. Sadikoglu, M. Ozdemir, and M. Seker. Optimal Control of the Primary Drying Stage of Freeze Drying of Solutions in Vials Using Variational Calculus. *Drying Technology*, 21(7):1307–1331, January 2003.
- [24] P. Sheehan and A. I. Liapis. Department of Chemical Engineering and Biochemical Processing Institute, University of Missouri- Rolla, Rolla, Missouri 65409-1230. 1998.
- [25] Salvatore A. Velardi and Antonello A. Barresi. Development of simplified models for the freeze-drying process and investigation of the optimal operating conditions. *Chemical Engineering Research and Design*, 86(1):9–22, January 2008.

Appendix A

Latent Heat Boundary Condition After Conformal Mapping

As mentioned before the derivation of the last boundary condition in the new plane, Z , consists of two parts. The rhs of the original equation needs to be rewritten w.r.t. X, Y , the new variables, and the partial derivative of Θ w.r.t. the normal on the interface is not the same in both planes. To this end let us first consider the partial derivatives of g_c , where g_c is the interface function in the corners. By the use of the chain rule we have:

$$\frac{\partial g_c}{\partial x^*} = \frac{\partial g_c}{\partial X} \frac{\partial X}{\partial x^*} + \frac{\partial g_c}{\partial Y} \frac{\partial Y}{\partial x^*} = 2x^* \frac{\partial g_c}{\partial X} + 2y^* \frac{\partial g_c}{\partial Y} \quad (\text{A.1})$$

$$\frac{\partial g_c}{\partial y^*} = \frac{\partial g_c}{\partial X} \frac{\partial X}{\partial y^*} + \frac{\partial g_c}{\partial Y} \frac{\partial Y}{\partial y^*} = -2x^* \frac{\partial g_c}{\partial Y} + 2y^* \frac{\partial g_c}{\partial X} \quad (\text{A.2})$$

By substituting (A1) and (A2) in the original rhs we get:

$$\begin{aligned} \text{rhs} &= -\frac{1}{2} \frac{2x^{*2} \frac{\partial g_c}{\partial X} + 2x^* y^* \frac{\partial g_c}{\partial Y} - 2y^{*2} \frac{\partial g_c}{\partial X} + 2x^* y^* \frac{\partial g_c}{\partial Y}}{\sqrt{4(x^{*2} + y^{*2}) \left(\frac{\partial g_c}{\partial X}\right)^2 + 4(x^{*2} + y^{*2}) \left(\frac{\partial g_c}{\partial Y}\right)^2}}, \\ &= -\frac{1}{2\sqrt{x^{*2} + y^{*2}}} \frac{(x^{*2} - y^{*2})g_{cX} + 2x^* y^* g_{cY}}{\sqrt{g_{cX}^2 + g_{cY}^2}}, \\ \text{rhs} &= -\frac{1}{2(X^2 + Y^2)^{1/4}} \frac{Xg_{cX} + Yg_{cY}}{\sqrt{g_{cX}^2 + g_{cY}^2}}. \end{aligned} \quad (\text{A.3})$$

The difference in the normal derivative after the conformal mapping can be found by making again use the chain rule.

$$dX = \frac{\partial X}{\partial x^*} dx^* + \frac{\partial X}{\partial y^*} dy^* = 2x^* dx^* - 2y^* dy^*$$

$$dY = \frac{\partial Y}{\partial x^*} dx^* + \frac{\partial Y}{\partial y^*} dy^* = 2y^* dx^* + 2x^* dy^*$$

As a result,

$$dX^2 + dY^2 = 4(x^{*2} + y^{*2})(dx^{*2} + dy^{*2})$$

Finally we know that $dN^2 = dX^2 + dY^2$ and $dn^2 = dx^{*2} + dy^{*2}$ and so we get,

$$dn = \frac{dN}{4\sqrt{X^2 + Y^2}} \quad (\text{A.4})$$

From (A3) and (A4) we can now write down the complete boundary condition in the Z plane as seen in the main text.

$$\frac{\partial \Theta}{\partial N} = -\frac{X g_{cX} + Y g_{cY}}{4(X^2 + Y^2)^{1/2} (g_{cX}^2 + g_{cY}^2)^{1/2}}. \quad (\text{A.5})$$

Appendix B

Leading Order Approximation of Integrals In The Two Limit Cases

Taking the imaginary part in the equation for $P(Z)$ we are left with an equation for $\Psi(X, Y)$ that involves integrals on a contour. As our goal was to find specific equation for Ψ on the boundaries, two limits were taken, $Y \rightarrow 0$ and $Y \rightarrow F(X)$. When considering these limiting cases caution is needed in order to find the correct leading term. The integrals involved in the in these equation can be divided into two, more general, categories.

$$\int_{-\infty}^{\infty} \frac{H(\xi)(\xi - X)}{(\xi - X)^2 + (Y - F(X))^2} d\xi, \quad (\text{B.1})$$

$$\int_{-\infty}^{\infty} \frac{H(\xi)(Y - F(X))}{(\xi - X)^2 + (Y - F(X))^2} d\xi. \quad (\text{B.2})$$

From the above general forms it is clear that the case where $Y \rightarrow 0$ is not a problem. This is not the case for $Y \rightarrow F(Y)$ where the effect is different for the two integrals. The first integral has a logarithmic dependence on X . It can be broken down into three integrals:

$$\int_{-\infty}^{X-\epsilon} \frac{H(\xi)}{\xi - X} d\xi + \int_{X-\epsilon}^{X+\epsilon} \frac{H(\xi)}{\xi - X} d\xi + \int_{X+\epsilon}^{\infty} \frac{H(\xi)}{\xi - X} d\xi.$$

Where $\epsilon \ll 1$. Taking the limit $\epsilon \rightarrow 0$ the middle integral becomes zero and the the rest two are the definition of a Principal value integral where the contribution comes from $H(\xi)$ throught the integral and is hence global.

$$\int_{-\infty}^{\infty} \frac{H(\xi)}{\xi - X} d\xi. \quad (\text{B.3})$$

For the second form the main contribution comes from $\xi \rightarrow X$ since there is no logarithmic dependence any more on X and the numerator goes to 0 as $Y \rightarrow F$. Consequently, to leading order, H can be taken out of the integral as $H(X)$ along with $Y-F$ and the integral can be evaluated.

$$H(X)(Y - F(X)) \int_{-\infty}^{\infty} \frac{1}{(\xi - X)^2 + (Y - F(X))^2} d\xi,$$

$$H(X)(Y - F) \frac{1}{Y - F} \int_{-\infty}^{\infty} \frac{1}{\left(\frac{\xi - X}{Y - F}\right)^2 + 1} d\xi,$$

$$H(X) \left[\tan^{-1} \left(\frac{\xi - X}{Y - F} \right) \right]_{-\infty}^{\infty},$$

$$H(X)\pi.$$

Hence the leading term.

Appendix C

Asymptotic Limits of Θ , Ψ On The Corner's Sides

In the small time regime the values for Θ , Ψ on the corners must approach asymptotically their values in the top and side thin layers. Having derived the equation for Θ for these regions, Ψ can be found using the Cauchy-Riemann equation in the z plane. For the top layer is used to give the equation for Ψ where $\Theta = -\frac{y^*}{\sqrt{2}}$ as found.

$$\frac{\partial \Psi}{\partial x^*} = \frac{1}{\sqrt{2}} \implies \Psi = \frac{x^*}{\sqrt{2}}.$$

For the side layers where Θ is given by $\Theta = -\frac{x^*}{\sqrt{2}}$ we use the second relation, $\Psi_{y^*} = \Theta_{x^*}$.

$$\frac{\partial \Psi}{\partial y^*} = \frac{1}{\sqrt{2}} \implies \Psi = \frac{y^*}{\sqrt{2}}.$$

In order to find the equation for Θ and Ψ in the Z plane we need to use the equations connecting X, Y with x^*, y^* but we need to be careful with so as to chose the correct sign. By solving the system of algebraic equation (1.6-1.7) w.r.t. y^* we arrive at two possible solutions:

$$y^* = \pm \frac{\sqrt{-X + \sqrt{X^2 + Y^2}}}{\sqrt{2}}.$$

To chose the correct sign we need the notice that y^* is negative since its sign is controlled by y -H which starts from 0 and goes to $-H$ for increasing time. Hence, the equation for the asymptotic solution of Θ in the Z plane as $X \rightarrow \infty$ is given by:

$$\Theta_{s1} = \frac{\sqrt{-X + \sqrt{X^2 + Y^2}}}{2}. \quad (\text{C.1})$$

The relevant equation for $X \rightarrow -\infty$ is given by solving for x^* initially or we can guess it intuitively since there is symmetry in the Z plane along the Y axis and hence Θ must be even.

$$\Theta_{s2} = \frac{\sqrt{X + \sqrt{X^2 + Y^2}}}{2}. \quad (\text{C.2})$$

The same holds for Ψ which can be found again using the Cauchy-Riemann equations.

$$\Psi_{s1} = -\frac{\sqrt{X + \sqrt{X^2 + Y^2}}}{2}, \quad (\text{C.3})$$

$$\Psi_{s2} = -\frac{\sqrt{-X + \sqrt{X^2 + Y^2}}}{2}. \quad (\text{C.4})$$